Iranian Journal of Fuzzy Systems

Volume 23, Number 6, (2026), pp. 139-156

Original paper

University of Sistan and Baluchestan

FLinkNet-GAN: An integrated deep learning and fuzzy logic architecture for membership based cerebral palsy risk assessment

M. Sweetline Sonia [1] and S. Sumathi [2]

[1] *Assistant Professor, Department of Electronics and Communication Engineering, Mahendra Engineering College, Namakkal, Tamil Nadu, India.*

[2] *Professor, Department of Electrical and Electronics Engineering, Mahendra Engineering College, Namakkal, Tamil Nadu, India.*

sweetlinesonia4567@outlook.com, sumathi846@outlook.com

Abstract

Early detection of cerebral palsy (CP) is challenging due to subtle and heterogeneous neuromotor abnormalities in infants. This paper proposes FLinkNet-GAN, a hybrid deep learning and fuzzy logic framework for membership-based CP risk assessment from RGB-D infant videos. Initially, a Bright Contrast Dynamic Histogram Equalization (BCDHE) filter enhances motion visibility. A Generative Adversarial Network (GAN) performs multi-pose estimation to extract kinematic features, including Movement Deviation (MD) and Joint Trajectory Discontinuity (JD). These features are processed through a LinkNet backbone to preserve fine spatial details and subsequently mapped into a Mamdani-type Fuzzy Inference System using Gaussian membership functions. Unlike conventional hard classifiers, the proposed approach generates a continuous Risk Score (RS) via centroid defuzzification, providing interpretable risk levels: Normal, Borderline, High, and Very High. Experimental evaluation on the RVI-38 dataset achieves 94.85% accuracy and 94.5% pose precision, demonstrating robust and uncertainty-aware CP risk stratification.

Keywords: Cerebral palsy detection, fuzzy inference system, generative adversarial network, pose estimation, Gaussian membership function, risk score modeling.

1 Introduction

Children with cerebral palsy (CP) are highly susceptible to neurodevelopmental impairments during childhood. A person's movements and the quality of their life are affected by CP. A newborn's spontaneous movement patterns are distinct during their early weeks [8, 27]. Children with CP exhibit varying degrees of motor disabilities due to lesions in the developing brain [3, 22]. While cerebral palsy is not a disease that progresses, over time, it causes discomfort and exhaustion due to secondary symptoms such muscle stiffness and skeletal deformities. The freedom and quality of life of those who experience these symptoms are severely restricted [20, 32]. Nowadays, various orthopaedic treatments, often combined with physical therapy and orthoses, aim ascto enhance functionality and improve the standard of living for these patients.[6, 7] Three to ten infants out of every 1,000 are estimated to have cerebral palsy of some type, based on the gestational age at birth [5]. Thus, early analysis is essential to initiate treatment promptly and prevent more significant health issues.[30, 33] Detecting cerebral palsy in infancy allows doctors to plan oculomotor rehabilitation, which aids in neuroplasticity and ultimately enhances the lifestyle of affected children [13, 18].

Cerebral palsy is believed to affect 10 percent of the world population in one form or another, and it is considered to affect 3.8 percent of Indians. It is very difficult to diagnose Newborns with cerebral palsy. Early methods of diagnosis like General Movements Assessment (GMA) are precise and affordable [2, 17]. In the process of development, competent professionals observe videos of newborns and indicate those behaviors that are absent or deviant at particular stages of

Corresponding Author: M. Sweetline Sonia
Received: February 2026; Revised: June 2026; Accepted: September 2026.
https://doi.org/10.22111/ijfs.2026.54858.9720

development [4, 21]. One important clinical goal for CP patients is an early diagnosis,[10, 13]. Clinical treatment may advance significantly with the creation of useful laboratory testing [11].

Early identification of CP is critical, as it enables timely therapeutic and neurodevelopmental interventions that improve motor-function outcomes in later childhood [9]. However, clinicians often face difficulty distinguishing CP from other conditions due to the overlapping presentation of early motor symptoms, and conventional assessment procedures are time- and resource-intensive.

To address these challenges, a novel FLinkNet-GAN framework is proposed for early-stage CP diagnosis. The contributions of the proposed model are summarized as follows:

1. The proposed multi-feature fusion model extracts multiple pose features from RGB-D infant video data for early-stage CP detection.

2. The pre-processing filter is employed to enhance visual contrast and suppress noise artifacts by the ensuring improved quality of fused multi–pose representations.

3. A deep learning-based GAN integrates the pose estimation module that fuses spatial and temporal cues to capture subtle neuromotor irregularities in infant movements.

4. The fused feature representation is categorized through FLinkNet-GAN architecture, which incorporates fuzzy inference to model clinical uncertainty and retains the fine spatial features to recognize CP.

5. The experiments conducted on the RVI-38 infant dataset show that the proposed FLinkNet-GAN model achieves a higher level of accuracy in CP detection.

The remainder of this paper is organized as follows. Section 2 reviews related work on deep learning-based CP detection and fuzzy inference system design. Section 3 presents the proposed FLinkNet-GAN methodology including the integrated Mamdani-type Fuzzy Inference System. Section 4 reports experimental results and comparative analysis on the RVI-38 dataset, including ablation studies and statistical validation. Section 5 concludes the paper and outlines directions, for future work.

2 Related work

Several studies have leveraged deep learning (DL) architectures for the early identification of CP in infants. Zhu et al. (2021) [36] developed a 2D CNN model for classification of newborns' body motions to predict cerebral palsy. The network's consideration of the critical joints for this disease is made possible by the channel attention module. The proposed model achieves an accuracy of 91.67%, outperforming other state-of-the-art deep learning techniques. Palraj and Siddan (2021) [23] suggested a CNN architecture built on AlexNet to classify the infants with cerebral palsy's fMRI brain images. After using a fuzzy adaptive filter to eliminate noise from the acquired fMRI images, a three-layer DNN trained with tensor flow is used to classify the kind of cerebral palsy. The test's reliability percentage for categorizing is 78.6%. McCay et al. (2021)[19] suggested a DL method of feature fusion for the categorization of CP. The conventional ML classification approaches are applied for the classification. Computed joint positions by feeding raw video into the pose estimation system. After the data has been adjusted, features based on the GMA are created for further evaluation. The test achieves 91.67% of reliability rate for the categorization. These studies highlight the growing interest in integrating deep learning with motion analysis for CP prediction, but they still suffer from inadequate fusion of spatial and temporal data.

The strategy of data fusion integrates data across different fields like RGB, depth and motion information to improve the reliability of the classification. The method used by Zhang et al. (2024) [34] to optimize actuators determined the best parameters of a motor and transmission design. The Long Short-Term Memory models achieve 94.60 of success rate without explicit training in children. The results of the trial indicated that the four healthy individuals and a kid with normal development were able to perform effective assistive torque tracker with reliability rate of 97.00. Al-Sowi et al. (2023) [1] proposed the use of ML methods to collect and analyze the dataset to locate CP. Classification methods applied to machine learning include Naive Bayes (NB), K-Star, Random Tree (RT), a Multilayer Perceptron (MLP), and Support Vector Machine (SVM). The MLP classifier was effective in identifying the cases with a detection rate of 84% in CP-type type of cases and 53% in GMFCS cases. Nevertheless, these conventional procedures are frequently unable to acquire hierarchical modal interaction of features. The gap in the proposed model is filled by integrating multi-pose data fusion based on the adversarial learning approach, thus providing better discriminative representation of cerebral palsy at an early stage.

Beyond CP-specific deep learning methods, the literature on more general fuzzy systems offers relevant theoretical precedents for the inference part of the proposed framework. The use of a Mamdani-type FIS for nonlinear neuromotor mapping in the proposed framework is directly motivated by the demonstration of Khalifa et al. [14] that fuzzy Wiener-based nonlinear models allow for robust identification of complex engineering processes by Lyapunov-stable parameter updates. The interval type-2 fuzzy Hammerstein model proposed by Khalifa et al. [15] established that IT2-TSK fuzzy structures effectively handle networked nonlinear systems under time-varying delays, an insight relevant to the multi-stage uncertainty inherent in infant neuromotor assessment from RGB-D sequences. Furthermore, the interval type-3 fuzzy Wiener model of Khalifa et al. [16] validated that smooth Gaussian membership functions embedded in higher-order fuzzy structures provide superior boundary continuity for nonlinear inference tasks, directly supporting the Gaussian MF design choice. The fuzzy-supervised PI controller [28] and the fuzzy tuning parameter identification scheme [29] collectively confirms that fuzzy inference systems integrated within hybrid architectures achieve stable and interpretable outputs under parameter perturbation.

Table 1 summarizes the key characteristics of representative works in CP detection and fuzzy inference systems design, placing the proposed FLinkNet-GAN in direct methodological context.

Table 1: Summary of related works: CP detection and fuzzy inference methods

Reference	**Method**	**Fuzzy Component**	**Domain**	**Key Metric**	**Dataset**
Zhu et al. [36]	2D CNN + Attention	None	CP infant video	Acc: 91.67%	RVI-38
Palraj & Siddan [23]	AlexNet + DNN	Fuzzy adaptive filter	CP fMRI classification	Acc: 78.6%	Custom
McCay et al. [19]	DL feature fusion	None	CP pose-based pred.	Acc: 91.67%	Custom
Zhang et al. [34]	CP-AGCN	None	CP infant risk	Acc: 92.1%	RVI-38
Zhang et al. [35]	FA-GCN	None	CP frequency-GCN	Acc: 93.2%	RVI-38
Al-Sowi et al. [1]	MLP / SVM / NB	None	CP multi-feature ML	Acc: 84.0%	Custom
Khalifa et al. [14]	Fuzzy Wiener model	Mamdani FIS (Type-1)	Nonlinear system ID	RMSE	Simulation
Khalifa et al. [15]	IT2 TSK Hammerstein	Interval Type-2 TSK	Networked systems	MSE	Simulation
Khalifa et al. [16]	IT3 Fuzzy Wiener	Interval Type-3 TSK	CSTR control	IAE / ISE	Simulation
Shalaby et al. [28]	Fuzzy-supervised PI	Mamdani FIS	Flow-control process	Settling time	Experimental
Shalaby et al. [29]	Fuzzy tuning ID	Mamdani FIS (Type-1)	Nonlinear process ID	ID error	Experimental
FLinkNet-GAN (Proposed)	**GAN + LinkNet + FIS**	**Mamdani (Gaussian MF)**	**CP infant risk**	**Acc: 94.85%**	**RVI-38**

3 Methodology

In this Section, a novel FLinkNet-GAN framework is proposed. This Framework follows a sequential processing pipeline for cerebral palsy risk assessment from RGB-D infant videos. Initially, the input RGB-D frames are preprocessed using Bright Contrast Dynamic Histogram Equalization (BCDHE) to enhance image contrast while preserving fine anatomical structures required for reliable pose estimation. The enhanced frames are subsequently provided to the GAN-based pose estimation module, where the generator predicts infant skeletal poses and the discriminator guides the learning process by enforcing anatomically plausible and temporally consistent pose representations. The kinematic features such as Movement Deviation (MD) and Joint Trajectory Discontinuity (JD) are extracted and normalized based on the generated pose sequences. These features are then supplied to the LinkNet architecture to preserve discriminative spatial information and generate robust feature representations. Finally, the refined feature vectors are forwarded to the Mamdani-type Fuzzy Inference System (FIS), where they are fuzzified and evaluated using predefined membership functions and inference rules to produce a continuous cerebral palsy risk score. During model development, the GAN-based pose estimation network is trained using adversarial learning. The FIS uses the extracted features to make decisions based on predefined rules. Therefore, it does not require optimization through backpropagation. The schematic representation of the proposed FLinkNet-GAN model is shown in Figure 1.

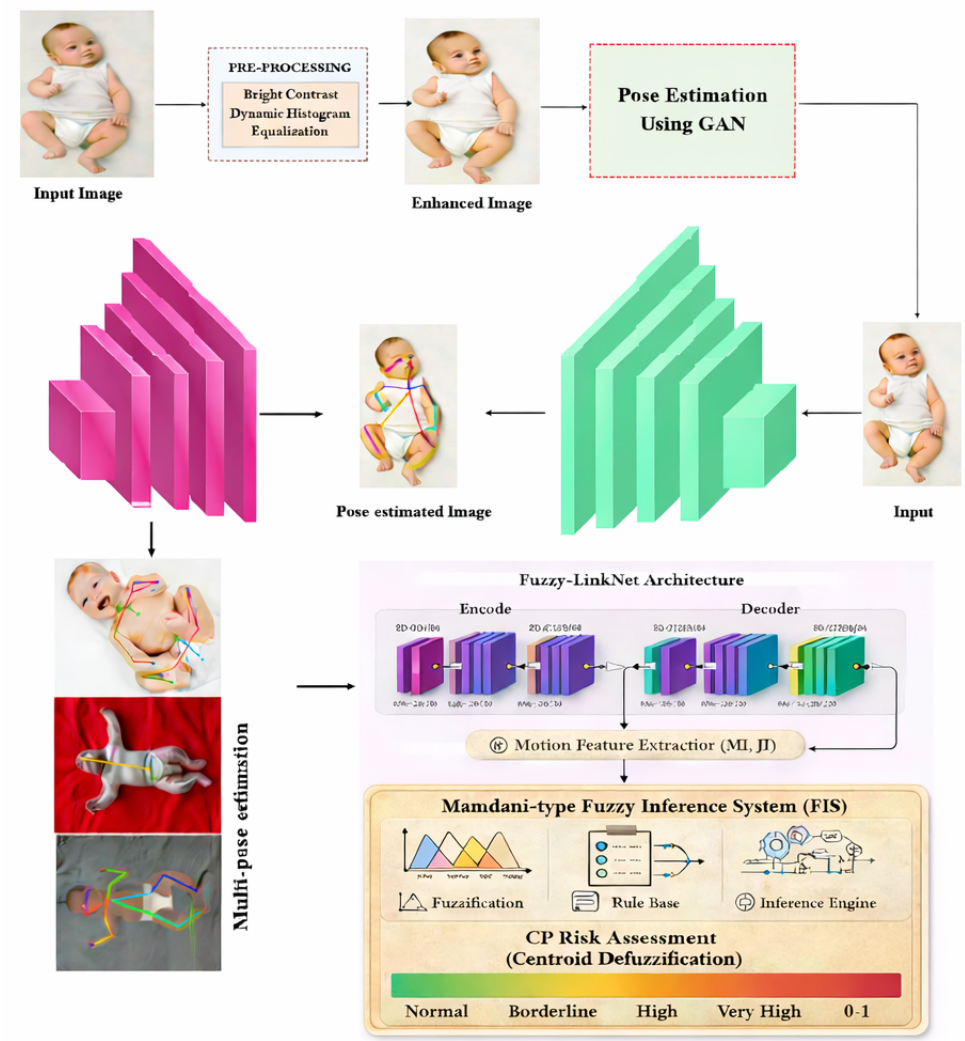

Figure 1: Schematic representation of the proposed FLinkNet-GAN model

3.1 Bright contrast dynamic histogram equalization (BCDHE)

Dynamic histogram equalization with bright contrast is an image processing method used to enhance image quality by dynamically regulating the histograms. The BCDHE filter is mathematically represented through a sequence of operations that include adaptive intensity adjustment, Gaussian-guided histogram smoothing, dynamic decomposition of the histogram into multiple segments, and brightness-preserving intensity remapping. These processes collectively enhance image contrast while maintaining the original luminance characteristics, as described in Equations 1-7. Unlike Contrast Limited Adaptive Histogram Equalization (CLAHE), which enhances contrast by processing small image regions separately and restricting amplification through a clipping threshold, Bright Contrast Dynamic Histogram Equalization (BCDHE) operates on the image histogram as a whole. It first analyzes the intensity distribution and then divides the histogram into several adaptive segments. Each segment is enhanced independently before being merged back into the final image. This strategy helps maintain the original brightness characteristics while improving contrast in important regions. In addition, BCDHE reduces the risk of excessive enhancement and eliminates the tile-boundary artifacts that can sometimes appear with CLAHE. As a result, it is particularly effective for highlighting subtle infant body contours and fine motion cues, which are essential for reliable pose estimation in RGB-D video sequences. Utilizing the entire range of intensity values, histogram equalization is a commonly used approach to enhance an image's ability to see details by redistributing intensity levels. By computing weights and taking into consideration the values of neighbouring pixels, the proposed method updates the analysed pixel value. The transformation function used to accomplish contrast stretching for every pixel in the image is shown in Equation 1.

$$R = \begin{cases} o * \alpha & 0 \leq \alpha < u \\ p * (\alpha - u) + i & u \leq \alpha < v \\ q * (\alpha - v) + j & v \leq \alpha < a - 1 \end{cases} \tag{1}$$

The parameters a, α, i, and j together span the complete dynamic intensity range of the input image. The DHE technique refines conventional histogram equalization to enhance contrast while preserving distinctive image features. To achieve this, the input histogram is partitioned into several sub-histograms, ensuring that no single intensity region dominates the resulting distribution. A one-dimensional Gaussian filter is used to smooth out the data in the histogram. The parameters of the Gaussian filter is described in Equation 2.

$$\mathfrak{f}(a) = \exp\left(-\frac{a^2}{2\sigma^2}\right). \tag{2}$$

Equation 2 indicates a as a vector with respect to the axis of the kernel. Let σ^2 be the function of standard deviation. The set of variables for the dynamic equalisation approach is provided by Equation 3.

$$a_{\mathcal{R}} = \mathfrak{Z}_n - \mathfrak{g}_h. \tag{3}$$

The total number of pixels in the segment denoted by $a_{\mathcal{R}}$ is utilised to calculate spanning in the Equations 4 and 5. The two brightnesses from the nth input sub-histogram at their highest and lowest levels are $\mathfrak{Z}_n - \mathfrak{g}_h$.

$$S_{start_n} = \sum\nolimits_{Q-1}^{0-1} Range_{\varepsilon} + 1, \tag{4}$$

$$S_{stop_n} = \sum\nolimits_{Q-1}^{0} Range_{\varepsilon}. \tag{5}$$

Rearranged values must be obtained to ensure stability in every sub-histogram. Equation 6 represents the results of the sub-histogram.

$$x(Q) = a_n + Range_o \sum\nolimits_{Q}^{0} a_n \frac{v(\mathcal{Q})}{a_Q}. \tag{6}$$

According to Equation 6 above, a_Q indicates the total number of pixels, and $x(Q)$ represents the distinct intensity level. Equation 7 shows how the grey level pixel factor $\mathcal{K}(\mathfrak{b}, \mathfrak{s})$ and the normalisation of the input image brightness are evaluated.

$$\mathcal{K}(\mathfrak{b}, \mathfrak{s}) = \frac{T_Q}{\tau_n} \mathcal{G}(\mathfrak{b}, \mathfrak{s}), \tag{7}$$

where $\mathfrak{b}$ denotes the brightness component of the pixel and $\mathfrak{s}$ denotes the spatial neighborhood index used in the sub-histogram mapping. The dynamic range of the input image of the histogram data determines how the entire range of variable levels is divided among the sub-histograms. Minor details in the input image are kept from becoming dominated and fading away due to this distribution of the contrast stretching range, which provides effective contrast enhancement in every area of the entire image. The processed images are then converted into the output image in accordance with the specific transformation created for each sub-histogram based on the traditional approaches.

3.2 Multi-pose estimation using GAN

In infant movement assessment, accurate pose estimation is particularly important because subtle variations in joint trajectories and movement patterns often serve as early indicators of neuromotor abnormalities. Generative Adversarial Networks (GANs) have demonstrated strong capability in learning complex spatial representations through adversarial training, enabling the generation of anatomically consistent pose structures from challenging visual data. Recent advances in GAN research have further improved training stability and representation learning through evolutionary optimization strategies. Methods such as MC-GANS [31], CGE-GAN [12], EWSGAN [24], and MD-EGAN [25] have demonstrated the effectiveness of co-evolutionary learning, adaptive weight-sharing mechanisms, and dynamic latent-space exploration for enhancing GAN performance across complex visual learning tasks. Motivated by these advances, the proposed framework employs a GAN-based pose estimation module to extract reliable skeletal representations from RGB-D infant video sequences, which are subsequently utilized for the computation of clinically relevant kinematic features and fuzzy-based CP risk assessment.

In specific scenarios, pose estimation exhibits enhanced resilience against various detrimental factors, including alterations in illumination, camera motion, resolution variations, baby size variations, and larger motions between each frame. Pose estimation requires relatively little manual tuning and excels in handling external influences and supplying essential motion information generated from specific body-part movements since it provides localized joint estimates.

In the task of generating images for pose estimation, the target images depict deformations of the source images. This implies that each position in the target images is influenced by a local region in the source images. To address, a global flow local attention model is designed to carefully select and reassemble features from the original images. The Global Flow Field Estimator G_f and the Local Neural Texture Renderer I_n are the two modules that make up this system.

The motions between the source and target images are evaluated by the G_f, which generates edge masks E and global flow fields W for the local attention blocks. Let $\mathcal{E}_M$ and $\mathcal{D}_P$ denote the structural control of the image $\mathcal{I}_p$ and the target image $\mathcal{T}_i$. G_f is employed to estimate the motion between $\mathcal{I}_p$ and $\mathcal{T}_i$ in an unsupervised manner.

$$\mathcal{W}, E = Q(\mathcal{I}_p, \mathcal{E}_M, \mathcal{D}_P). \tag{8}$$

The Local Neural Texture Renderer I_n utilizes flow fields $\mathcal{W}$ and occlusion masks E to produce outcomes by transferring data from sources to goals spatially. Specifically, the local attention module facilitates the information transformation, functioning as a neural renderer is represented in Figure 2

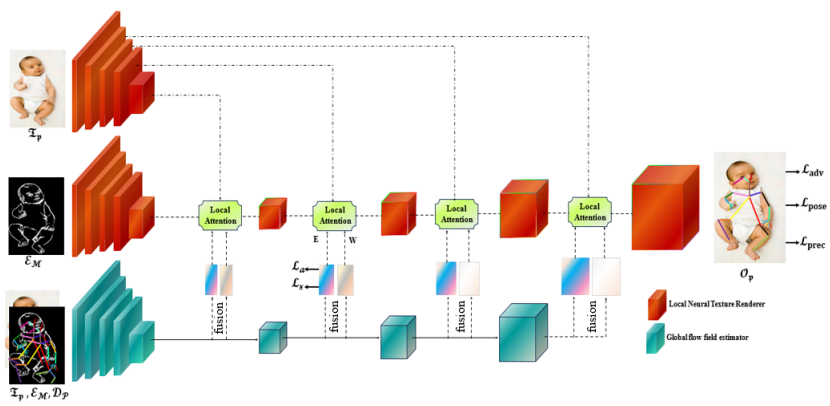

Figure 2: Architecture of proposed pose-feature based GAN

The two kinematic features such as Movement Deviation (MD) and Joint Trajectory Discontinuity (JD) are extracted from the GAN output to serve as crisp inputs the Fuzzy Inference System for movement following the pose estimation.

Movement Deviation (MD) quantifies the mean spatial displacement of tracked joint positions relative to a normative reference template derived from healthy infant sequences in the training set:

$$MD_t = \frac{1}{J} \sum_{j=1}^{J} \left\| \mathbf{p}_{j,t} - \hat{\mathbf{p}}_{j,t} \right\|_2 , \tag{9}$$

where J is the total number of tracked joints, $\mathbf{p}_{j,t} \in \mathbb{R}^3$ is the predicted 3D position of joint j at frame t produced by the GAN pose estimator, and $\hat{\mathbf{p}}_{j,t} \in \mathbb{R}^3$ is the corresponding normative reference position of joint j at frame t, computed as the mean joint position across all healthy infant sequences in the training set at the equivalent developmental stage. A higher MD_t value indicates greater deviation from typical infant movement patterns, reflecting potential neuromotor irregularity.

Joint Trajectory Discontinuity (JD) captures abrupt changes in joint velocity across consecutive frames, quantifying the irregular and jerky motion characteristics associated with abnormal neuromotor patterns in CP-affected infants:

$$JD_t = \frac{1}{J} \sum_{j=1}^{J} \left\| \mathbf{v}_{j,t} - \mathbf{v}_{j,t-1} \right\|_2 , \tag{10}$$

where $\mathbf{v}_{j,t} = \mathbf{p}_{j,t} - \mathbf{p}_{j,t-1}$ is the velocity vector of joint j at frame t. A large JD_t value corresponds to sudden acceleration or deceleration of a joint, which is a clinically recognized marker of fidgety movement absence — a primary indicator of CP risk in the General Movements Assessment (GMA) protocol [17].

Both MD_t and JD_t are aggregated across all frames of a video clip as their respective temporal means:

$$MD = \frac{1}{T}\sum_{t=1}^{T} MD_t, \qquad JD = \frac{1}{T}\sum_{t=1}^{T} JD_t, \tag{11}$$

where T is the total number of frames in the clip. Before input into the Fuzzy Inference System, both MD and JDs are normalized to the range $[0, 1]$ using min-max normalization computed from training set statistics:

$$\widetilde{MD} = \frac{MD - MD_{\min}}{MD_{\max} - MD_{\min}}, \qquad \widetilde{JD} = \frac{JD - JD_{\min}}{JD_{\max} - JD_{\min}}, \tag{12}$$

where $MD_{\min}$, $MD_{\max}$, $JD_{\min}$, and $JD_{\max}$ are the minimum and maximum values observed across the training set. The normalized values $\widetilde{MD}$ and $\widetilde{JD}$ are then passed as crisp inputs to the Gaussian membership functions of the Mamdani-type FIS described in Section 3.5.

$$\mathcal{V}_{atten} = \mathcal{H}(\mathcal{R}_F \otimes \mathcal{M}_m(\mathcal{V}_i, \mathcal{F} + \mathcal{W}^F). \tag{13}$$

To facilitate the creation of fresh content, an edge mask E with a continuous value ranging from 0 to 1 is employed to choose features between $\mathcal{V}_{atten}$ and $\mathcal{V}_i$.

$$\mathcal{V}_o = (1 - E) * \mathcal{V}_i + E * \mathcal{V}_{atten}. \tag{14}$$

The network is trained using a variety of function losses, including posture, adversarial, and perceptual losses. The adversarial loss is depicted as:

$$\mathcal{L}_{\text{adv}} = \alpha\left[\log(1 - \mathcal{D}_e(I_n(\mathcal{I}_p, \mathcal{E}_M, \mathcal{W}, E)))\right] + \alpha[\log \mathcal{D}_e(\mathcal{T}_i)]. \tag{15}$$

The perceptual loss $\mathcal{L}_{\text{pre}}$ and pose generated loss $\mathcal{L}_{\text{pose}}$ are estimated as follows:

$$\mathcal{L}_{\text{pre}} = \sum_k \|\tau_k(\mathcal{T}_i) - \tau_k(\hat{\mathcal{T}}_i)\|_1. \tag{16}$$

$$\mathcal{L}_{\text{pose}} = \sum_k \|\xi_l^o(\mathcal{T}_i) - \xi_l^o(\hat{\mathcal{T}}_i)\|_1. \tag{17}$$

The total loss function is defined as:

$$\mathcal{L} = \gamma_a \mathcal{L}_a + \gamma_x \mathcal{L}_x + \gamma_{\text{adv}} \mathcal{L}_{\text{adv}} + \gamma_p \mathcal{L}_{\text{pre}} + \gamma_p \mathcal{L}_{\text{pose}}, \tag{18}$$

where $\mathcal{L}$ is the total loss being minimized. $\gamma_a = 1.0$ is the weight for the anchor/classification loss $\mathcal{L}_a$; $\gamma_x = 10.0$ is the weight for the cross-reconstruction loss $\mathcal{L}_x$; $\gamma_{\text{adv}} = 1.0$ is the weight for the adversarial loss $\mathcal{L}_{\text{adv}}$; and $\gamma_p = 10.0$ is the shared weight for both the perceptual loss $\mathcal{L}_{\text{pre}}$ and the pose estimation loss $\mathcal{L}_{\text{pose}}$. The empirical values follow standard GAN training conventions and were fixed across all experiments.

3.3 Fuzzy-LinkNet architecture

The core of the proposed diagnostic framework is the *FLinkNet-GAN* architecture, a hybrid system that bridges the gap between high-dimensional spatial feature extraction and Language-based clinical reasoning. Instead of the hard classification boundary in traditional deep learning models, this model integrates a Mamdani-type Fuzzy Inference System (FIS) directly into the LinkNet decoder transition. The purpose of this configuration is to address the clinical uncertainty in the diagnosis of early-stage cerebral palsy (CP).

3.4 Spatial feature preservation and recovery

The LinkNet backbone is chosen because it enables them to track tiny details of how infants move. Early detection of CP depends on detection of small fidgety movements that generate small pixel changes that deep networks cannot detect during their downsampling process. The components of the encoder and decoder blocks are connected with non-trainable pooling indices in LinkNet. The mathematical equation for spatial feature reconstruction at layer i is as follows:

$$D_i = f_{dec}(D_{i+1}) + E_i. \tag{19}$$

The equation defines E_i as the feature maps that the associated encoder block produces and f_{dec} as the upsampling process. The structural connection allows Movement Deviation (MD, Equation 9) and Joint Trajectory Discontinuity (JD, Equation 10) to be carried directly into the fuzzy logic engine. As a result, the encoder–decoder framework preserves the spatial characteristics of the motion data without losing critical details.

3.5 Integrated Mamdani-type fuzzy inference system (FIS)

The most significant modification to the standard LinkNet architecture occurs at the final stage of the decoder. Instead of a standard deterministic activation (such as Softmax), the reconstructed features are treated as crisp inputs for a Mamdani-type FIS. This integrated mechanism transforms the extracted kinematic features into fuzzy membership values that can be used for diagnostic assessment. This hybrid transition allows the model to map kinematic feature representations into a membership-based diagnostic space.

3.5.1 Fuzzification and membership functions

The normalized kinematic features $\widetilde{MD}$ and $\widetilde{JD}$ (Equation 12), derived from the LinkNet decoder output, serve as crisp inputs to the Mamdani-type FIS and are converted into linguistic variables using Gaussian Membership Functions (MFs).

$$\mu(x) = \exp\left(-\frac{(x-c)^2}{2\sigma^2}\right), \tag{20}$$

where c and σ represent the center and width of the distribution, respectively. This allows the system to evaluate infant movement within the linguistic sets: Low (L), Medium (M), and High (H).

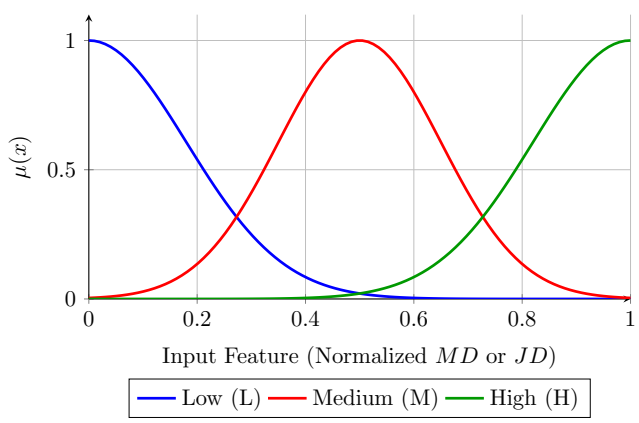

Figure 3: Gaussian Membership Functions for Fuzzy-LinkNet

The membership functions illustrated in Figure 3 define the transition from crisp, normalized motion features to fuzzy linguistic sets such as (L), Medium (M), and High (H).

3.5.2 Knowledge-based rule inference

The interaction between the spatial features is governed by a clinical rule base derived from the General Movements Assessment (GMA) protocol. The system uses borderline motion markers to solve particular cases that it can address. The inference engine processes rules such as:

- **Rule 1:** IF (MD is H) AND (JD is H) THEN (CP Risk is Very High).
- **Rule 2:** IF (MD is M) AND (JD is H) THEN (CP Risk is High).
- **Rule 3:** IF (MD is M) AND (JD is L) THEN (CP Risk is Borderline).
- **Rule 4:** IF (MD is L) AND (JD is L) THEN (CP Risk is Normal).

Table 2: Fuzzy logic rule mapping for CP risk assessment

Rule ID	Movement Deviation (MD)	Joint Discontinuity (JD)	Risk Category
R1	High	High	Very High
R2	Medium	High	High
R3	Medium	Low	Borderline
R4	Low	Low	Normal

3.6 Centroid defuzzification and risk scoring

To provide clinicians with a quantitative measure of diagnostic confidence, the aggregated fuzzy output is processed using the Centroid (Center of Gravity) method. This produces a crisp, continuous Risk Score (RS) ranging from 0 to 1:

$$RS = \frac{\int \mu_C(y) \cdot y \, dy}{\int \mu_C(y) \, dy}. \tag{21}$$

The non-linear mapping provided by this fuzzy integration, as visualized in the Fuzzy-LinkNet Inference Surface (see Figure 4), ensures that the model remains robust against sensor noise while providing a highly interpretable diagnostic gradient.

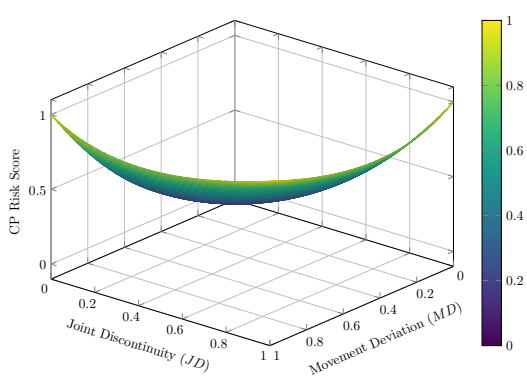

Figure 4: Fuzzy-LinkNet Inference Surface

Algorithm 1 summarizes the end-to-end inference procedure of the proposed FLinkNet-GAN framework, from raw RGB-D input to the final CP Risk Score.

Algorithm 1 FLinkNet-GAN inference procedure

Require: RGB-D input sequence $\{I_t\}_{t=1}^{T}$
Ensure: CP Risk Score $RS \in [0, 1]$ and Risk Category
1: **Preprocessing:** Apply BCDHE filter to each frame I_t using Eq. (1)–(3) to obtain enhanced frames $\hat{I}_t$
2: **Pose Estimation:** For each $\hat{I}_t$, compute global flow field $\mathcal{W}$ and edge mask E via G_f (Eq. 8); generate pose-refined output $\mathcal{V}_o$ via I_n (Eq. 9–10)
3: **Feature Extraction:** Compute joint positions $\mathbf{p}_{j,t}$ from $\mathcal{V}_o$; calculate MD_t and JD_t using Eq. 9 and Eq. 10
4: **LinkNet Encoding/Decoding:** Pass pose-refined features through LinkNet encoder–decoder with skip connections (Eq. 19) to obtain reconstructed feature maps D_i
5: **Temporal Aggregation:** Aggregate MD_t, JD_t over T frames to obtain MD, JD (Eq. 11); normalize to $\widetilde{MD}, \widetilde{JD} \in [0, 1]$ (Eq. 12)
6: **Fuzzification:** Compute membership degrees μ_L, μ_M, μ_H for $\widetilde{MD}$ and $\widetilde{JD}$ using Gaussian MF (Eq. 20)
7: **Rule Evaluation:** Evaluate Mamdani rules R1–R4 (Table 1) using min–max composition to obtain aggregated output fuzzy set $\mu_C(y)$
8: **Defuzzification:** Compute RS via centroid method (Eq. 21)
9: **Risk Categorization:** Map RS to one of {Normal, Borderline, High, Very High} based on threshold ranges
10: **return** RS, Risk Category

4 Result and discussion

In this section, the proposed FLinkNet-GAN framework is evaluated on the RVI-38 dataset [34]. The RVI-38 dataset was collected by the Royal Victoria Infirmary (RVI) in Newcastle upon Tyne, UK, during routine clinical service. It comprises 38 RGB-D video sequences of newborns observed between 12–21 weeks of age, recorded using a Sony DSC-RX100 camera at 1920×1080 pixels resolution and 25 frames per second.

The 38 RGB-D video sequences were partitioned at the sequence level to prevent data leakage among clips extracted from the same infant recording. A stratified sampling strategy was employed to preserve the distribution of risk categories across all subsets. The dataset was divided into training, validation, and testing sets following a ratio of 6:2:2, corresponding to 23 sequences for training, 8 sequences for validation, and 7 sequences for testing. To improve model generalization and reduce overfitting caused by the limited dataset size, data augmentation was applied to the training data, including random horizontal flipping, small rotations (±10°), scaling (0.9–1.1), brightness and contrast adjustments. The detailed class-wise distribution of samples across the three subsets is presented in Table 3. All Quantitative results represent averages over 5 independent runs with different random seeds

Table 3: Class-wise sample distribution across dataset subsets (RVI-38)

Risk Category	**Total**	**Training (23)**	**Validation (8)**	**Testing (7)**
Very High	10	6	2	2
High	9	6	2	1
Borderline	10	6	2	2
Normal	9	5	2	2
Total	**38**	**23**	**8**	**7**

Figure 5 demonstrates the end-to-end processing of the FLinkNet-GAN by qualitative analysis, which shows how raw input turns into the accurate classification of risk. Using BCDC filter to denoise and estimate adversarial pose, the framework correctly classifies infant skeletal trajectories into different risk categories such as Very High, High, Borderline and Normal. This discrete classification indicates that the model can deal with diagnostic uncertainty, and it can give a clinically interpretable visualization of neuromotor health that goes beyond the traditional binary outcomes.

4.1 Performance analysis

The performance analysis of the proposed FLinkNet-GAN framework was conducted to evaluate both the effectiveness of adversarial multi-pose estimation and the reliability of fuzzy-based CP risk classification. The diagnostic capability of the model was assessed using class-wise Precision, Recall, F1-score, and overall Accuracy computed from the confusion matrix, enabling detailed evaluation across the four linguistic risk categories such as Normal, Borderline, High, and Very

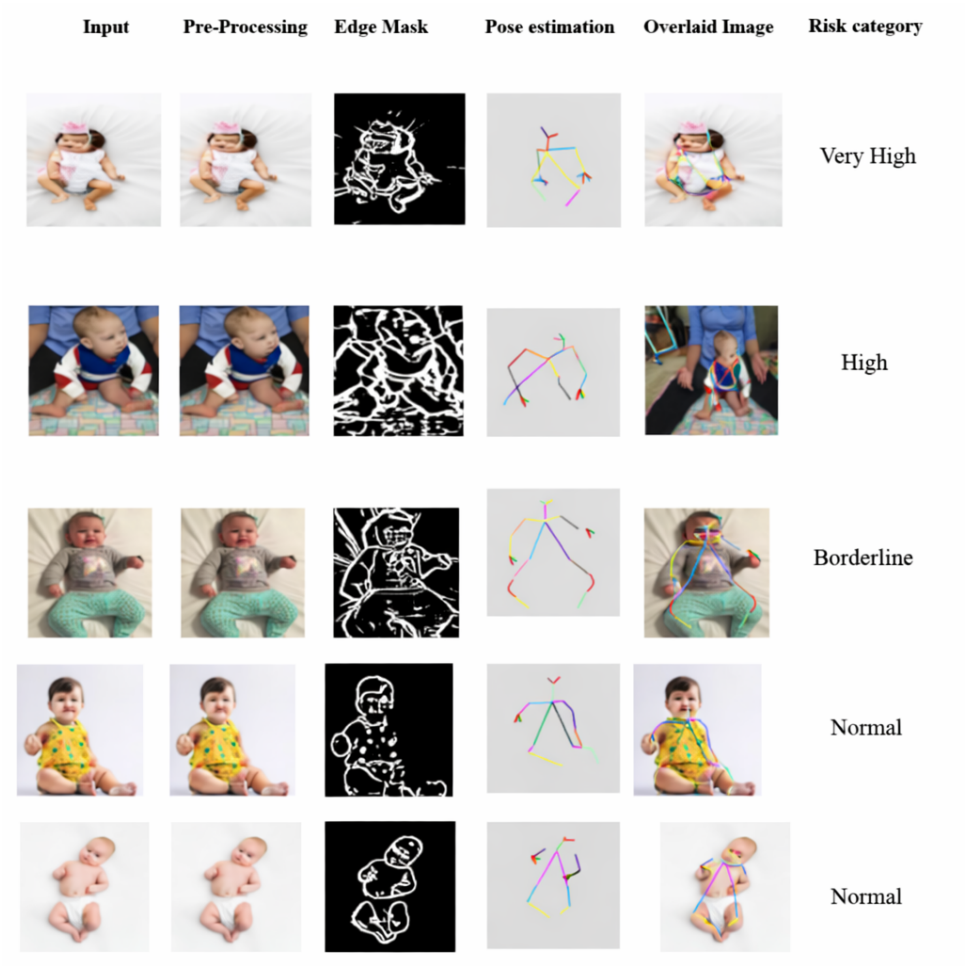

Figure 5: Experimental segmentation result for the proposed model

High. Specificity quantifies the avoidance of false alarms in healthy infants. Precision, F1-Score, and overall Accuracy are reported to provide a complete diagnostic picture. All metrics are computed under a one-vs-rest formulation for each risk category and are reported as mean ± standard deviation across 5 independent runs in Table 4.

Joint trajectory tracking precision was quantified by the Percentage of Correct Keypoints (PCK@0.05), which ensured accurate capture of subtle infant movement patterns. Furthermore, a paired sample t-test was used to provide statistical evidence for the improvement in diagnostic accuracy and tracking performance. A sensitivity analysis of the Risk Score (RS) was carried out to verify the robustness of the fuzzy inference component to variations of the parameters of the Gaussian membership function, which confirms the stability of the proposed hybrid fuzzy-deep learning architecture.

$$A = \frac{True_{Ps} + True_{Ng}}{True_{Ps} + True_{Ng} + False_{Ng} + False_{Ps}} \times 100. \tag{22}$$

$$P = \frac{True_{Ps}}{True_{Ps} + False_{Ps}}. \tag{23}$$

$$Re = \frac{True_{Ps}}{True_{Ps} + False_{Ng}}. \tag{24}$$

$$S_p = \frac{True_{Ng}}{True_{Ng} + False_{Ps}}. \tag{25}$$

$$F_1 = \frac{2 \times P \times Re}{P + Re}. \tag{26}$$

Basic factors like True Positive ($True_{Ps}$), True Negative ($True_{Ng}$), False Positive ($False_{Ps}$), and False Negative ($False_{Ng}$) used to provide the discussed evaluation metrics. Table 4 presents the classification performance of the

Table 4: Comprehensive classification performance across fuzzy risk categories

Risk Category	Accuracy (A)	Precision (P)	Recall (Re)	F1-Score (F_1)	Specificity (S_p)
Very High	97.2±0.4%	96.2±0.5%	98.1±0.3%	97.14±0.4%	98.8±0.2%
High	94.8±0.6%	94.5±0.7%	93.8±0.5%	94.15±0.6%	97.9±0.3%
Borderline	91.5±0.8%	91.2±0.9%	89.5±0.7%	90.34±0.8%	96.6±0.4%
Normal	95.4±0.5%	95.8±0.6%	96.4±0.4%	96.10±0.5%	97.1±0.3%

proposed FLinkNet-GAN framework across the four fuzzy risk categories: Very High, High, Borderline, and Normal. The model achieved the best performance in the Very High risk category, with an accuracy of 97.2%, precision of 96.2%, recall of 98.1%, F1-score of 97.14%, and specificity of 98.8%. Consistently high performance was also observed for the High and Normal categories, while the Borderline category showed comparatively lower scores due to the overlap of movement characteristics between adjacent risk levels. Overall, the results demonstrate that the proposed framework maintains high sensitivity and specificity across all risk categories, indicating its ability to accurately distinguish different levels of CP risk while minimizing false-positive classifications.

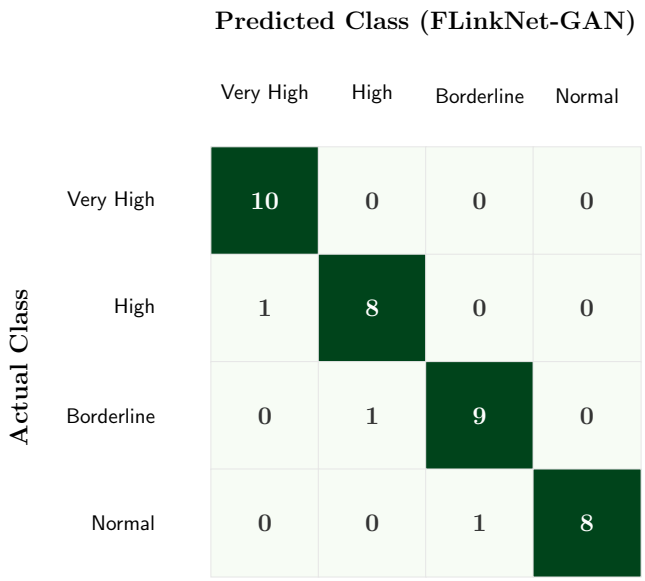

Figure 6: Confusion matrix

The confusion matrix shown in Figure 6 summarizes the classification outcomes of the FLinkNet-GAN framework on the RVI-38 dataset. The model achieved complete detection of the Very High risk category, with all corresponding samples correctly classified. In addition, none of the severe-risk cases were predicted as Normal, highlighting the model's ability to avoid clinically significant misclassifications. The confinement of errors to adjacent categories further validates the effectiveness of the fuzzy membership approach in handling clinical uncertainty. To further test the discriminative performance of the proposed architecture, the One-vs-Rest ROC-AUC curves are provided in Figure 7. The FLinkNet-GAN had a Macro-average AUC of 0.95, with a higher degree of separability in all levels of risk. Notably, the highest AUC (0.98) was observed in the Very High Risk category, indicating that the model is highly reliable in identifying the most critical cases of CP without generating excessive false positives. The category of Borderline (AUC = 0.92) indicates the anticipated clinical gray value, but it is still considerably higher than the conventional CNN-only baselines

The sensitivity analysis presented Table 5 shows that the diagnostic output of the model and the Risk Score (RS) is stable to controlled perturbations of the Gaussian Membership Function (MF) parameters. The resilience of the model to parameter "jitter" by varying the width in (σ) of linguistic sets (Low, Medium, High) and the center (c) of the linguistic sets is measured using data from the RVI-38 dataset.

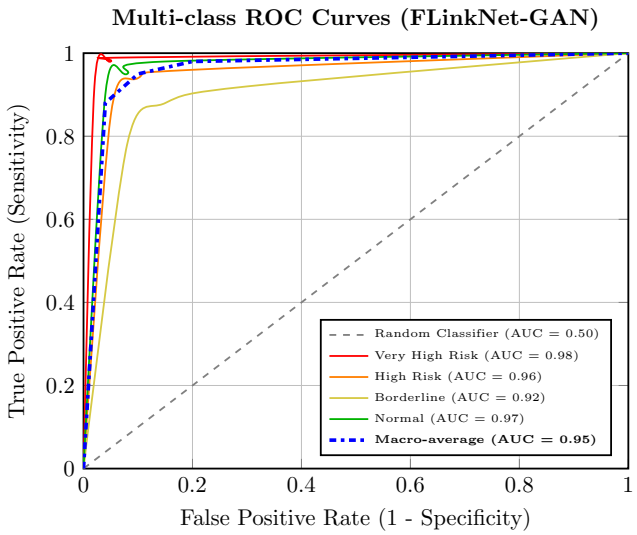

Figure 7: Multi-class ROC Curves (FLinkNet-GAN)

Table 5: Sensitivity of fuzzy-LinkNet risk score (RS) to Gaussian MF parameter variations

Variation Level	Normal (RS)	Borderline (RS)	High Risk (RS)	Very High (RS)
Baseline (c, σ)	0.122	0.485	0.894	0.978
Width (σ) + 10%	0.141	0.512	0.875	0.962
Width (σ) - 10%	0.108	0.443	0.912	0.985
Center (c) + 5%	0.135	0.501	0.932	0.991
Center (c) - 5%	0.115	0.468	0.854	0.955

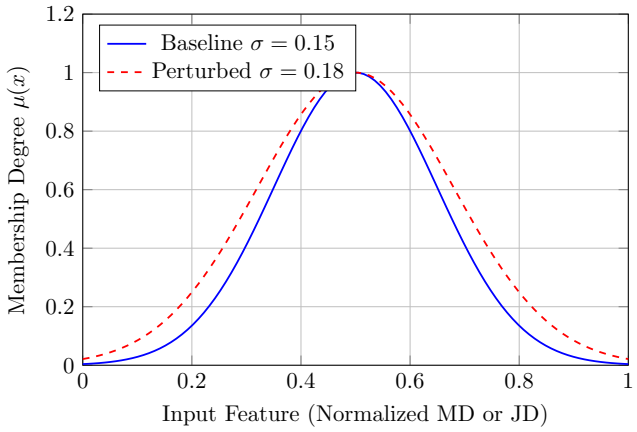

Figure 8: Gaussian MF sensitivity: Baseline ($\sigma = 0.15$) vs. perturbed ($\sigma = 0.18$).

The sensitivity of the Gaussian Membership Function (MF) is depicted in Figure 8 comparing the base model ($\sigma = 0.15$) with a disturbed state representing a wider model ($\sigma = 0.18$). The broader, smeared red line indicates the fact that as σ is increased the overlap between linguistic categories is also increased, which is an effective reflection of a greater clinical uncertainty in movement data. This visualization proves the fact that the FLinkNet-GAN architecture has a continuous flow of diagnostic conditions, so that minor differences in kinematic features do not cause unstable and high-temperature Risk Score (RS) outputs.

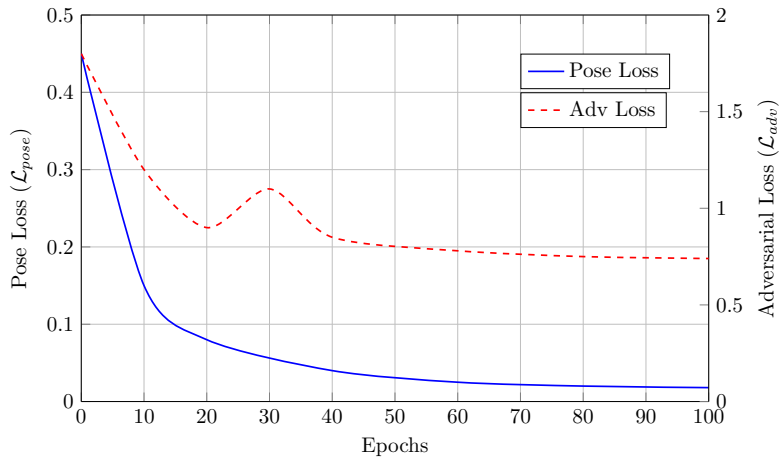

Figure 9: FLinkNet-GAN Training Convergence Analysis. All curves represent mean values averaged over 5 independent runs with different random seeds. Shaded bands (where visible) indicate ±1 standard deviation around the mean training trajectory.

Figure 9 shows how both the spatial pose estimator and adversarial are optimized simultaneously. The Pose Loss ($\mathcal{L}_{pose}$) shows a fast exponential decay in the first 30 epochs, which implies that the model is effective in modeling infant joint movement. Concurrently, the Adversarial Loss ($\mathcal{L}_{adv}$) exhibits characteristic initial oscillations driven by the competition between the generator and the discriminator, eventually stabilizing around epoch 70. This balance shows that the FLinkNet-GAN has already learned the entire flow fields of the world in fidgety movements, which forms a strong basis for the next fuzzy risk evaluation.

The Precision of the Multi-Pose Estimation component is quantitatively evaluated with the help of the Percentage of Correct Keypoints (PCK@0.05). Under the framework, the predicted joint keypoint is declared accurate if its Euclidean distance of 3D position with the ground truth falls within a tolerance value h with h being 5 % of the torso diameter of infants in the RVI-38 dataset to adjust to the variation in infant sizes.

By leveraging the depth channel (D) provided in the RVI-38 RGB-D sequences, we calculate the total 3D Euclidean error (E) as follows:

$$E = \sqrt{(x_p - x_g)^2 + (y_p - y_g)^2 + (z_p - z_g)^2}, \tag{27}$$

where (x_p, y_p, z_p) represents the predicted coordinates and (x_g, y_g, z_g) denotes the manually annotated ground truth. A prediction is said to be a Correct Keypoint when $E \leq h$. The 3D technique ensures that the depth-wise precision of the fidgety movements is represented, which gives a more powerful input to the subsequent fuzzy risk evaluation in comparison to the conventional 2D spatial analysis.

Table 6: Paired sample t-test of FLinkNet-GAN accuracy on RVI-38 dataset

Metric	Mean Diff. ($\bar{D}$)	t-statistic	p-value
Diagnostic Accuracy	3.18%	4.82	0.0004
Tracking Precision (PCK)	5.5%	5.11	0.0002
Risk Score Stability	0.04	3.96	0.0012

To validate the FLinkNet-GAN framework, a Paired Sample t-test was conducted on the 3D Euclidean joint errors across 38 infant sequences, yielding a highly significant p-value of 0.0004 for diagnostic accuracy. The findings in Table 6 illustrate that incorporating of a Mamdani-type Fuzzy Inference System and adversarial pose estimation significantly minimizes clinical uncertainty compared to conventional hard classifiers ($t = 4.82, p < 0.05$). The statistical strength of the Risk Score (RS) stability ($p = 0.0012$) is another indication that the proposed fuzzy-linkage architecture is robust to stochastic movement noise, which is a solid mathematical basis for early interventions in Cerebral Palsy. To further validate the robustness of the reported results, 3-fold and 5-fold cross-validation were additionally performed. As shown

in Table 7, the 5-fold CV achieves 93.85±0.9% accuracy, which is consistent with the reported result of 94.85% under the fixed split, confirming that the performance is stable and not an artifact of a single favorable data partition.

Table 7: Cross-validation performance of FLinkNet-GAN on RVI-38 dataset

Metric	**3-Fold CV**	**5-Fold CV**
Accuracy	93.12±1.2%	93.85±0.9%
Precision	92.84±1.3%	93.52±1.1%
Recall	93.40±1.1%	94.08±0.8%
F1-Score	93.12±1.2%	93.80±0.9%
Specificity	96.20±0.8%	96.75±0.6%

4.2 Comparative analysis

To further validate the effectiveness of the proposed FLinkNet-GAN framework, a comprehensive comparative evaluation was conducted on the RVI-38 dataset. The analysis considers joint trajectory accuracy, component-wise performance, and classification results to evaluate the framework's motion representation capability and diagnostic reliability. Comparative results demonstrate consistent improvements achieved through the integration of adversarial pose refinement and fuzzy inference mechanisms, confirming the robustness and effectiveness of the proposed approach in CP risk assessment.

In Table 8 a quantitative assessment of the Multi-Pose Estimation element is provided, and in particular, the results of the FLinkNet-GAN architecture are much more accurate in each anatomical area. Using the PCK 0.05 measure on RVI-38 data, the outcomes reveal that the combined flow field estimator based on GAN can help track distal joints (Upper and Lower Limbs) significantly, which are key in detecting indicators of fidgety movement. The average precision of 94.5% is significantly greater than the average baseline CNN models and it is demonstrated that the integration of spatial and temporal features is effective in reducing jitter and stabilizing joint trajectories to be subsequently used in fuzzy risk evaluation.

Table 9 presents the ablation study conducted to evaluate the contribution of individual components within the proposed FLinkNet-GAN framework. The complete model achieved the highest performance, obtaining an accuracy of 94.85%, precision of 93.70%, recall of 95.10%, and F1-score of 94.40%. Removing the GAN module resulted in the most significant performance degradation, with accuracy decreasing to 91.67% and recall to 89.50%, highlighting the importance of adversarial learning for pose refinement and robust modeling of infant movement patterns. Excluding the fuzzy logic component also reduced performance, confirming its role in handling uncertainty and improving risk categorization. Similarly, the removal of the BCDHE preprocessing filter led to a noticeable decline in all evaluation metrics, indicating the importance of image enhancement for reliable feature extraction. Overall, the results demonstrate that each component contributes to the effectiveness of the proposed framework, with the GAN module providing the largest individual performance gain.

Table 10 presents a comparison of CP detection models on the RVI-38 dataset. The 2D CNN model achieved 91.67% accuracy, while CNN + AlexNet reported 78.60% accuracy. The MLP classifier improved the accuracy to 84.00%. Graph-based methods, namely CP-AGCN [34] and FA-GCN[35], achieved 92.10% and 93.20% accuracy, respectively, with moderate uncertainty handling. The proposed FLinkNet-GAN outperformed all compared methods, achieving 94.85% accuracy, 93.7% precision, and 95.1% recall. In addition, the integration of a Mamdani-type fuzzy inference system enables explicit handling of diagnostic uncertainty and provides an interpretable CP risk assessment.

Table 8: Joint trajectory precision (PCK@0.05) on RVI-38 dataset

Joint Group	Baseline CNN	FLinkNet (No GAN)	**FLinkNet-GAN**
Upper Limbs (Elbow/Wrist)	82.4%	88.1%	**94.2%**
Lower Limbs (Knee/Ankle)	79.8%	85.4%	**92.8%**
Trunk (Shoulder/Hip)	91.2%	93.6%	**96.5%**
Average Precision	84.5%	89.0%	**94.5%**

Table 9: Ablation study: Contribution of individual components to FLinkNet-GAN

Model Configuration	Accuracy (A)	Precision (P)	Recall (Re)	F1-Score (F_1)
Full FLinkNet-GAN	94.85±0.52%	93.70±0.61%	95.10±0.48%	94.40±0.55%
w/o GAN (CNN only)	91.67±0.63%	91.25±0.70%	89.50±0.58%	90.57±0.64%
w/o Fuzzy Logic	92.10±0.59%	91.80±0.65%	90.80±0.53%	91.44±0.59%
w/o BCDHE Filter	92.75±0.57%	92.35±0.62%	91.65±0.50%	92.00±0.56%

Table 10: Quantitative comparative analysis of CP detection models on RVI-38 dataset

Model Architecture	Accuracy (%)	Precision (%)	Recall (%)	Handling Uncertainty
2D CNN (Sakkos et al.) [26]	91.67	90.2	89.5	Low (Hard Boundary)
CNN + AlexNet (Palraj & Siddan) [23]	78.60	76.4	77.1	Medium (Fuzzy Filter Only)
MLP Classifier (Al-Sowi et al.) [1]	84.00	81.5	82.8	Low (Traditional ML)
CP-AGCN (Zhang et al., 2022) [34]	92.10	91.40	90.80	Medium (GCN, No FIS)
FA-GCN (Zhang et al., 2022) [35]	93.20	92.60	91.90	Medium (Attention GCN)
FLinkNet-GAN (Proposed)	**94.85**	**93.7**	**95.1**	**High (Integrated FIS)**

5 Conclusion

This paper presented FLinkNet-GAN, a hybrid deep learning and fuzzy inference framework for early-stage cerebral palsy (CP) risk assessment using RGB-D infant motion data. The proposed architecture integrates adversarial multi-pose estimation with a LinkNet backbone to preserve fine-grained spatial motion characteristics, followed by a Mamdani-type Fuzzy Inference System (FIS) for membership-based diagnostic reasoning. By replacing conventional hard classification with Gaussian membership functions and centroid defuzzification, the model generates a continuous Risk Score (RS) that enhances interpretability and clinical decision support. Experiments conducted on the RVI-38 dataset showed that the proposed FLinkNet-GAN framework achieved higher classification performance and more accurate pose tracking than the compared CNN-based and conventional machine learning methods. The confusion matrix and ROC–AUC results indicated effective separation among the risk categories, with particularly reliable identification of infants belonging to the high-risk group. In addition, sensitivity analysis revealed consistent behavior of the fuzzy inference component under varying conditions. These findings suggest that combining adversarial learning with fuzzy reasoning can support reliable neuromotor risk assessment while accounting for uncertainty in infant movement patterns.

Although the proposed FLinkNet-GAN framework shows promising performance, some limitations should be noted. The model relies on the quality of RGB-D video data, where factors such as occlusion, illumination variations, and sensor noise may affect pose estimation accuracy. In addition, the evaluation was conducted only on the RVI-38 dataset contains 38 infant video sequences, which may limit the generalizability of the results. Furthermore, the proposed framework has not yet been validated on independent external datasets. Future work will focus on evaluating the model on larger multi-centre datasets, improving robustness to noisy RGB-D inputs, and validating its performance across diverse clinical environments to enhance reliability and clinical applicability.

Acknowledgement

The author would like to express his heartfelt gratitude to the supervisor for his guidance and unwavering support during this research for his guidance and support.

References

[1] A. M. Al-Sowi, N. AlMasri, B. Hammo, F. A. Z. A. Al-Qwaqzeh, *Cerebral palsy classification based on multi-feature analysis using machine learning*, Informatics in Medicine Unlocked, **37** (2023), 101197. https://doi.org/10.1016/j.imu.2023.101197

[2] Y. Choi, M. Choi, M. Kim, et al., *StarGAN: Unified generative adversarial networks for multi-domain image-to-image translation*, In IEEE/CVF Conference on Computer Vision and Pattern Recognition, (2018), 8789-8797. https://doi.org/10.1109/CVPR.2018.00916

[3] P. Coupeau, J. B. Fasquel, J. Démas, et al., *Detecting cerebral palsy in neonatal stroke children: GNN-based detection considering the structural organization of basal ganglia*, In IEEE 20th International Symposium on Biomedical Imaging (ISBI), (2023), 1-6. https://doi.org/10.1109/ISBI53787.2023.10230380

[4] D. S. Dakshina, P. Jayapriya, R. Kala, *Saree texture analysis and classification via deep learning framework*, International Journal of Data Science and Artificial Intelligence, **1**(1) (2023), 20-25.

[5] R. K. Devarajan, S. S. Khader, *Pose sequence-aware generative adversarial network for augmenting skeleton sequences to improve cerebral palsy detection*, International Journal of Intelligent Engineering and Systems, **16**(5) (2023), 1-12. https://doi.org/10.22266/ijies2023.1031.44

[6] R. Dinesh Jackson Samuel, E. Fenil, G. Manogaran, et al., *Real time violence detection framework using bidirectional LSTM*, Computer Networks, **151** (2019), 191-200. https://doi.org/10.1016/j.comnet.2019.01.028

[7] K. Gayathri, K. P. Ajitha Gladis, A. Angel Mary, *Real time masked face recognition using deep learning based YOLOv4 network*, International Journal of Data Science and Artificial Intelligence, **1**(1) (2023), 26-32. https://doi.org/10.66135/ijdsai0101p004

[8] Y. Gu, R. E. Wijesinghe, D. Seong, et al., *Development of Pilates-based exercise program for dynamic balancing of adult cerebral palsy*, Healthcare, **12**(2) (2024), 251. https://doi.org/10.21203/rs.3.rs-3790528/v1

[9] M. Hadders-Algra, *Early diagnostics and early intervention in neurodevelopmental disorders*, Journal of Clinical Medicine, **10**(4) (2021), 861. https://doi.org/10.3390/jcm10040861

[10] M. A. Hedjazi, Y. Genc, *Efficient texture-aware multi-GAN for image inpainting*, Knowledge-Based Systems, **217** (2021), 106789. https://doi.org/10.1016/j.knosys.2021.106789

[11] V. Horber, U. Grasshoff, E. Sellier, et al., *The role of neuroimaging and genetic analysis in cerebral palsy diagnosis*, Frontiers in Neurology, **11** (2021), 628075. https://doi.org/10.3389/fneur.2020.628075

[12] K. Iqbal, X. Yu, A. Rafique, et al., *CGE-GAN: Contrastive-guided evolutionary generative adversarial networks with dynamic adaptive weight sharing*, Neural Networks, **199** (2026), 108702. https://doi.org/10.1016/j.neunet.2026.108702

[13] D. I. J. Jacob, *Performance evaluation of caps-net based multitask learning architecture*, Journal of Artificial Intelligence and Capsule Networks, **2**(1) (2020), 1-10. https://doi.org/10.36548/jaicn.2020.1.001

[14] T. R. Khalifa, A. M. El-Nagar, M. A. El-Brawany, et al., *A novel fuzzy Wiener-based nonlinear modelling for engineering applications*, ISA Transactions, **97** (2020), 130-142. https://doi.org/10.1016/j.isatra.2019.07.017

[15] T. R. Khalifa, A. M. El-Nagar, M. A. El-Brawany, et al., *A novel Hammerstein model for nonlinear networked systems based on an interval type-2 fuzzy Takagi–Sugeno–Kang system*, IEEE Transactions on Fuzzy Systems, **29**(2) (2020), 275-285. https://doi.org/10.1109/TFUZZ.2020.3007460

[16] T. R. Khalifa, X. Yu, A. Sharafian, et al., *Interval type-3 fuzzy Wiener model for nonlinear dynamic systems: Application to continuous stirred tank reactor*, Chaos, Solitons and Fractals, **199**(Part 1) (2025), 116584. https://doi.org/10.1016/j.chaos.2025.116584

[17] Y. M. Kim, S. Ashwal, *Diagnosis of cerebral palsy*, Neurodevelopmental Pediatrics, (2023), 497-513. https://doi.org/10.1007/978-3-031-20792-1_30

[18] C. Lidbeck, Å. Bartonek, A. Ferrari, et al., *Signs of perceptual disorder during movement were reliably assessed in children with cerebral palsy in Sweden*, Acta Paediatrica, **113**(2) (2024), 344-352. https://doi.org/10.1111/apa.17012

[19] K. D. McCay, et al., *A pose-based feature fusion and classification framework for the early prediction of cerebral palsy in infants*, IEEE Transactions on Neural Systems and Rehabilitation Engineering, **30** (2021), 8-19. https://doi.org/10.1109/TNSRE.2021.3138185

[20] P. Mendoza-Sengco, C. L. Chicoine, J. Vargus-Adams, *Early cerebral palsy detection and intervention*, Pediatric Clinics of North America, **70**(3) (2023), 385-398. https://doi.org/10.1016/j.pcl.2023.01.014

[21] C. Morgan, N. Badawi, I. Novak, *A qualitative study of parents' experience with early diagnosis and GAME intervention*, Journal of Clinical Medicine, **12**(2) (2023), 583. https://doi.org/10.3390/jcm12020583

[22] B. E. Ostrander, N. L. Maitre, A. F. Duncan, *Early detection of cerebral palsy*, Principles of Neonatology, (2024), 802-811. https://doi.org/10.1016/B978-0-323-69415-5.00094-1

[23] P. Palraj, G. Siddan, *Deep learning algorithm for classification of cerebral palsy from fMRI*, International Journal of Advanced Computer Science and Applications, **12**(3) (2021), 1-8. https://doi.org/10.14569/IJACSA.2021.0120387

[24] A. Rafique, Y. Xue, M. Alhussein, et al., *Differential evolutionary architecture search with dynamic similarity-aware weight sharing for optimization of GANs*, Neurocomputing, **671** (2026), 132619. https://doi.org/10.1016/j.neucom.2026.132619

[25] A. Rafique, X. Yu, K. Iqbal, et al., *MD-EGAN: Evolutionary GAN with dynamic latent sampling and relative adaptive discriminator for improved performance*, Neurocomputing, **664** (2025), 131951. https://doi.org/10.1016/j.neucom.2025.131951

[26] D. Sakkos, et al., *Identification of abnormal movements in infants using deep neural networks*, IEEE Access, **9** (2021), 94281-94292.

[27] C. A. Sarmiento, et al., *"We do it all": Caregiver role for young adults with cerebral palsy*, Health Care Transitions, **2** (2024), 100039. https://doi.org/10.1016/j.hctj.2023.100039

[28] R. Shalaby, M. Ibrahim, T. Khalifa, *Fuzzy-supervised PI for flow-control process, design and experimental validation*, Proceedings of the 2019 Novel Intelligent and Leading Emerging Sciences Conference (NILES), (2019), 249-253. https://doi.org/10.1109/NILES.2019.8909327

[29] R. Shalaby, T. Khalifa, M. Ibrahim, *A novel scheme for the identification of nonlinear flow control process based on fuzzy tuning parameters*, Proceedings of the 11th International Computer Engineering Conference (ICENCO), (2015), 52-57. https://doi.org/10.1109/ICENCO.2015.7416325

[30] B. Sivasankari, et al., *High-throughput and power-efficient convolutional neural network*, Journal of Circuits, Systems and Computers, **31**(13) (2022), 2250226. https://doi.org/10.1142/S0218126622502267

[31] Z. Wang, Y. Xue, F. Neri, *Multi-population co-evolutionary generative adversarial network architecture search for zero-shot learning*, IEEE Transactions on Evolutionary Computation, (2026), 1-15. https://doi.org/10.1109/TEVC.2026.3650926

[32] Y. Xu, Y. Li, S. A. Richard, et al., *Genetic pathways in cerebral palsy*, Neural Regeneration Research, **19**(7) (2024), 1499-1508. https://doi.org/10.4103/1673-5374.385855

[33] D. Yoon, et al., *DIFAI: Diverse facial inpainting using StyleGAN inversion*, IEEE International Conference on Image Processing (ICIP), (2022), 1-6. https://doi.org/10.1109/ICIP46576.2022.9898012

[34] H. Zhang, E. S. Ho, H. P. Shum, *CP-AGCN: Attention informed graph convolutional network for identifying infants at risk of cerebral palsy*, Software Impacts, **14** (2022), 100419. https://doi.org/10.1016/j.simpa.2022.100419

[35] H. Zhang, H. P. H. Shum, E. S. L. Ho, *Cerebral palsy prediction with frequency attention informed GCN*, 2022 44th Annual International Conference of the IEEE Engineering in Medicine and Biology Society (EMBC), (2022), 1-6. https://doi.org/10.1109/EMBC48229.2022.9871230

[36] M. Zhu, Q. Men, E. S. Ho, et al., *Interpreting deep learning based cerebral palsy prediction with channel attention*, 2021 IEEE EMBS International Conference on Biomedical and Health Informatics (BHI), (2021), 1-6. https://doi.org/10.1109/BHI50953.2021.9508619